
On the Bell–Plesset Effects: The Effects of Uniform Compression and Geometrical Convergence on the Classical Rayleigh–Taylor Instability

Introduction

This article considers a simple treatment of the Rayleigh–Taylor (RT) instability of incompressible perturbations of the interface between two homogeneous fluids undergoing acceleration due to a pressure gradient, including the effects of uniform compression and geometrical convergence. The growth rate for incompressible linear perturbations of a planar interface between incompressible fluids is well known from the work of Rayleigh¹ and Taylor² and has become a classic textbook result.^{3,4} When the perturbed interface undergoes compression or geometrical convergence, such as in the case of an interface embedded in a collapsing cylinder or sphere, the perturbation growth is modified. These modifications have been referred to collectively^{5,6} as Bell–Plesset (BP) effects.^{7,8} Both RT and BP effects are known to be important to the outcome of implosion experiments in inertial confinement fusion (ICF).^{9–11} The purpose of this article is to formulate and analyze BP effects in a simple way that reveals a wide range of behavior in a variety of geometries.

The term “accelerationless growth” has also been used for BP effects. This terminology acknowledges that interface perturbations would evolve due to convergence and compression in the absence of the buoyant force that drives the RT instability, but, as will be shown below, the modified RT growth does not separate naturally into an acceleration-driven RT contribution and an accelerationless contribution. Nevertheless, the chosen formulation clarifies the physical distinction between RT and BP effects. To be precise, the term “accelerationless” will be used below only to denote perturbation growth in the limit of no RT growth.

The description developed in this article is based on the very similar methods of Bell² and Plesset,³ combining Plesset’s treatment of interfaces with an arbitrary density jump, rather than only free surfaces, and Bell’s inclusion of uniformly compressible background flow. We also adopt Bell’s choice of a mass perturbation amplitude in order to obtain perturbation equations of a particularly simple and useful form. In cases where the local convergence and compression rates are con-

stant over useful time intervals, the perturbation solutions evolve exponentially, and scaling of the perturbation with the interface density and radius can be derived.

The Background Flow

To begin the perturbation calculation describing RT growth, we postulate one-dimensional irrotational unperturbed background flow in planar, cylindrical, and spherical geometries where an interface separates homogeneous fluids of contrasting uniform densities $\rho_1(t)$ and $\rho_2(t)$. The interface is at coordinate position $R(t)$, and the subscripts 1 and 2 denote the half-spaces at coordinate values less than or greater than $R(t)$, respectively. The fluid motion is fully specified by the interface history $R(t)$ and the rate of compression $\gamma_\rho(t)$. From this point on, $R(t)$, $\gamma_\rho(t)$, and other functions of time alone will be written without explicitly indicating the time dependence. This rate of compression is assumed to apply everywhere, or, in other words,

$$\gamma_\rho = \dot{\rho}_1/\rho_1 = \dot{\rho}_2/\rho_2. \quad (1a)$$

Similarly, the convergence rate is written as

$$\gamma_R = \dot{R}/R. \quad (1b)$$

For the cylindrical and spherical cases, R is the radius of the surface, while for a planar interface, the radius is effectively infinite, and $\gamma_R = 0$.

The unperturbed flow velocity is

$$v(x, t) = -(x - R)\gamma_\rho + \dot{R} \quad (2a)$$

in planar geometry,

$$v(r, t) = \dot{R}\left(\frac{R}{r}\right) + \left(\frac{\gamma_\rho}{2}\right)\left(\frac{R^2}{r^2} - 1\right)r \quad (2b)$$

in cylindrical geometry, and

$$v(r,t) = \dot{R} \left(\frac{R^2}{r^2} \right) + \left(\frac{\gamma_\rho}{3} \right) \left(\frac{R^3}{r^3} - 1 \right) r \quad (2c)$$

in spherical geometry. These velocities can be derived from the velocity potential functions

$$\Phi(x,t) = \Phi_0(t) - (x - R)\dot{R} + (x - R)^2 \gamma_\rho / 2 \quad (3a)$$

in planar geometry,

$$\Phi(r,t) = \Phi_0(t) - \left(R\dot{R} + \gamma_\rho R^2 / 2 \right) \ln r + \left(\gamma_\rho / 4 \right) r^2 \quad (3b)$$

in cylindrical geometry, and

$$\Phi(r,t) = \Phi_0(t) + \frac{R^2 \dot{R}}{r} + \left(\frac{\gamma_\rho}{3} \right) \left(\frac{r^2}{2} + \frac{R^3}{r} \right) \quad (3c)$$

in spherical geometry using

$$\vec{v} = -\vec{\nabla}\Phi \cdot \vec{e}_r \quad (4)$$

These flows can be obtained from the Euler equation in one dimension

$$\frac{\partial v}{\partial t} + v \frac{\partial v}{\partial x} = -\frac{\partial U(x)}{\partial x} - \frac{1}{\rho} \frac{\partial p(x,t)}{\partial x}, \quad (5)$$

given the appropriate pressure $p(x,t)$ and external potential field $U(x,t)$. In planar geometry, it is easy to verify that the desired flow is obtained from the pressure

$$p(x,t) = p_0 - \rho g_P (x - R) + \rho (\dot{\gamma}_\rho - \gamma_\rho^2) (x - R)^2 / 2 \quad (6a)$$

and the external potential field

$$U(x,t) = U_0 - g_U x, \quad (7)$$

where

$$g_P = -\frac{1}{\rho} \frac{\partial p(R,t)}{\partial x}$$

and

$$g_U = -\frac{\partial U(R)}{\partial x}$$

are the separate components of the fluid acceleration at the unperturbed interface position due to pressure and the external potential, respectively. Using

$$\dot{R} = v(R,t), \quad (8)$$

the Euler equation gives

$$\ddot{R} = g_U + g_P. \quad (9)$$

In cylindrical geometry, the required combination of pressure and potential field is

$$\begin{aligned} U + \frac{p}{\rho} &= \left(U + \frac{p}{\rho} \right)_{r=R} - \left[R\ddot{R} + \dot{R}^2 + \gamma_\rho R\dot{R} \right] \ln r \\ &\quad + \left[\frac{\dot{\gamma}_\rho}{2} - \left(\frac{\gamma_\rho}{2} \right)^2 \right] r^2 \\ &\quad - \frac{1}{2} \left[\frac{\dot{R}^2}{2} + \gamma_\rho R\dot{R} - \left(\frac{\gamma_\rho}{2} \right)^2 R^2 \right] \left(\frac{R^2}{r^2} \right), \end{aligned} \quad (6b)$$

and in spherical geometry, the required combination is

$$\begin{aligned} U + \frac{p}{\rho} &= \left(U + \frac{p}{\rho} \right)_{r=R} + \frac{\ddot{R}R^2}{r} - \left(\frac{2R\dot{R}^2}{r} - \frac{4}{3}\gamma_\rho \frac{R^2\dot{R}}{r} \right) \\ &\quad \times \left(1 - \frac{R^3}{4r^3} \right) - \left(\frac{\gamma_\rho}{3} \right)^2 \frac{r^2}{2} \left(1 - \frac{R^3}{r^3} \right)^2 \\ &\quad + \left(\frac{\dot{\gamma}_\rho}{3} \right) \frac{r^2}{2} \left(1 + \frac{2R^3}{r^3} \right). \end{aligned} \quad (6c)$$

Again, in both the latter cases, Eq. (9) is obtained from the Euler equation.

The one-dimensional background flow in planar geometry conserves mass everywhere according to

$$\vec{\nabla} \cdot \vec{v} = -\gamma_\rho, \quad (10a)$$

but, for arbitrary convergence and compression rates, a line source is required for cylindrical flow,

$$\vec{\nabla} \cdot \vec{v} = -\gamma_\rho + \dot{m}\delta^{(2)}(r), \quad (10b)$$

where

$$\frac{\dot{m}}{\pi\rho R^2} = 2\gamma_R + \gamma_\rho, \quad (11a)$$

and a point source is required for spherical flow,

$$\vec{\nabla} \cdot \vec{v} = -\gamma_\rho + \dot{m}\delta^{(3)}(r), \quad (10c)$$

where

$$\frac{3\dot{m}}{4\pi\rho R^2} = 3\gamma_R + \gamma_\rho. \quad (11b)$$

The cylindrical and spherical velocities given by Eqs. (2b) and (2c) can be written simply in terms of \dot{m} as

$$v(r,t) = \frac{\dot{m}}{2\pi r \rho} - \gamma_\rho \frac{r}{2} \quad (12a)$$

and

$$v(r,t) = \frac{\dot{m}}{4\pi r \rho^2} - \gamma_\rho \frac{r}{3}. \quad (12b)$$

To consider a broad range of BP effects, it is important to be able to specify the compression and convergence rates independently, and this requires the mass source \dot{m} at $r = 0$. Imposing $\dot{m} = 0$ restricts the problem to either constant cylindrical mass, $2\gamma_R + \gamma_\rho = 0$, or constant spherical mass, $3\gamma_R + \gamma_\rho = 0$. According to Eqs. (6), placing a mass source at $r = 0$ to create desired background flows introduces unphysical pressures at $r = 0$. These flows are unlikely to resemble any intended application globally, but they suffice for the perturbation calculations if they are reasonably descriptive of conditions in the neighborhood of the density jump because discrepant

flow beyond a few perturbation wavelengths from the density jump will be largely decoupled from the perturbations.

It is worth noting a curious property of Eq. (6a) for the pressure driving the planar flow. For planar flow that is either converging or diverging at a constant rate $\gamma_\rho = 0$, the pressure does not depend on the sign of γ_ρ ; in both cases, the pressure driving the flow exerts a diverging force, even if the flow is converging. In both cases, the distinction between diverging and converging flow comes from the initial conditions of the flow, not the pressure.

Perturbation Equations

To obtain the equations of motion for the incompressible perturbations of these interfaces, we follow the calculation of Plesset for a spherical interface.⁸ Following the work of Bell,⁷ we generalize Plesset's method to include cylindrical and planar geometries and to include compression of the unperturbed background flow at a spatially uniform rate.

The velocity potential function Φ describing irrotational flow with uniform mass density is governed by the Bernoulli theorem^{4,12}

$$\frac{p}{\rho} + U + \frac{1}{2}|v|^2 - \frac{\partial\Phi}{\partial t} = 0, \quad (13)$$

where all the quantities have been defined above. The velocity potential includes the potential for the background flow plus the potential perturbation $\Phi_{\text{total}} = \Phi + \phi_\ell(\vec{x},t)$. The subscript ℓ denotes the harmonic order of the perturbation mode corresponding to $\cos(2\pi\ell y/L)$, $\cos(\ell\theta)$, or $Y_\ell^m(\theta, \phi)$ transverse harmonic dependence in planar, cylindrical, and spherical geometry, respectively. The perturbation is assumed to be incompressible, which requires

$$\nabla^2 \phi_\ell = 0. \quad (14)$$

Imposing vanishing boundary conditions on ϕ_ℓ at large distances from the interface and continuity at the origin, if applicable, we obtain solutions for each side of the interface for planar, cylindrical, and spherical geometries:

$$\phi_{\ell\pm}(\vec{x},t) = b_{\ell\pm}(t)e^{\pm 2\pi\ell x/L} \cos(2\pi\ell y/L), \quad (15a)$$

$$\phi_{\ell\pm}(\vec{x},t) = b_{\ell\pm}(t)r^{\pm\ell} \cos(\ell\theta), \quad (15b)$$

and

$$\phi_{\ell\pm}(\vec{x}, t) = b_{\ell\pm}(t)r^{[\ell, -(\ell+1)]}Y_\ell^m(\theta, \phi). \quad (15c)$$

For the planar perturbation, we have imposed a zero boundary condition at $y = 0$ and $y = L$ so that the set of perturbation modes would form a discrete spectrum with an integer index ℓ , preserving a unity of notation among the three geometries with no loss of generality. For planar and cylindrical geometry, we have disregarded z -dependent perturbations.

The position of the perturbed interface is $r = r_s(t)$, where

$$r_s(t) = R + a_\ell(t) \cos(2\pi\ell y/L), \quad (16a)$$

$$r_s(t) = R + a_\ell(t) \cos(\ell\theta), \quad (16b)$$

and

$$r_s(t) = R + a_\ell(t)Y_\ell^m(\theta, \phi) \quad (16c)$$

for planar, cylindrical, and spherical geometries, respectively. The interface displacement a_ℓ is the spatial amplitude of the perturbation.

Whenever it is clear in the following development that a coordinate-dependent expression applies to all three geometries, the symbol r will be used to denote the coordinate in the direction of the unperturbed flow, rather than repeat the exact same expression using the Cartesian coordinate symbol x for planar flow.

An ordinary second-order differential equation for a_ℓ is obtained from Eq. (13), first by evaluating P on both sides of the interface in terms of the perturbed velocity potential to first order in small distances from the unperturbed interface. These expressions for P are then matched at the interface $r = r_s$. A required expression for the function $b_{\ell\pm}$ in terms of the amplitude a_ℓ is obtained by equating the interface velocity to the fluid velocity at the interface:

$$\frac{dr_s}{dt} = -\frac{\partial[\Phi(r_s, t) + \phi_{\ell\pm}(r_s, t)]}{\partial r}. \quad (17)$$

This matching of pressures eliminates δp_ℓ , leaving an ordinary homogeneous second-order differential equation for a_ℓ .

Equations (6) show that one can write a pressure that produces the desired background flow. For the purposes of constructing linear equations for flow perturbations near $r = R$, the linear approximation

$$U(x, t) \approx U_0 - rg_U, \quad p(x, t) \approx p_0 - (r - R)\rho g_p \quad (18)$$

suffices. As Eq. (9) for the interface acceleration suggests, the background flow does not depend on the potential and the pressure gradients separately, only their sum. The RT growth rate, however, depends most directly on g_p and not g_U . In the absence of pressure gradients $g_p = 0$, the fluid is in a state of free fall, where there are no buoyant forces to drive the RT instability.

To begin constructing the expression for pressure continuity at the perturbed interface, we begin by rewriting Eq. (13) as

$$\frac{P(r, t) + \delta p_\ell}{\rho} = -U_0 + rg_U - \frac{1}{2}|v|^2 + \frac{\partial \Phi}{\partial t}. \quad (19)$$

All quantities are evaluated at $r = r_s$ by expanding them to first order in the perturbation about the unperturbed interface position $r = R$. We evaluate the pressures in the fluid half-spaces $r < R$ and $r > R$, denoted by subscripts 1 and 2, respectively. Matching the harmonic components of the pressure perturbation $\delta p_{\ell 1} = \delta p_{\ell 2}$ gives the perturbation equations, which are

$$\left(-\gamma_\rho + \frac{d}{dt}\right) \frac{d}{dt}(a_\ell \rho) = \gamma_0^2(a_\ell \rho), \quad (20a)$$

$$\left(-\gamma_\rho + \frac{d}{dt}\right) \frac{d}{dt}(a_\ell \rho R) = \gamma_0^2(a_\ell \rho R), \quad (20b)$$

and

$$\left(-\gamma_\rho - \gamma_R + \frac{d}{dt}\right) \frac{d}{dt}(a_\ell \rho R^2) = \gamma_0^2(a_\ell \rho R^2) \quad (20c)$$

for planar, cylindrical, and spherical geometry, respectively. The resulting perturbation equations assume this simple and transparent form when written in terms of the “mass” amplitude z_ℓ , where

$$z_\ell = a_\ell \rho, \quad z_\ell = a_\ell \rho R, \quad \text{or} \quad z_\ell = a_\ell \rho R^2 \quad (21)$$

for the three chosen geometries. The interface density ρ can be the mean density $\rho = (\rho_1 + \rho_2)/2$ or any other fixed linear combination of ρ_1 and ρ_2 . Since a uniform compression rate applies everywhere, according to Eq. (1a), the only effect of alternative choices for the interface density is to introduce a constant factor into the definition of the mass amplitude [Eq. (21)]. The units of z_ℓ are mass only for spherical geometry. They are mass per area for planar geometry and mass per axial length for cylindrical geometry. In this form, the “driving” terms are proportional to the RT growth rates γ_0 , where

$$\gamma_0^2 = k \frac{(\rho_2 - \rho_1)}{(\rho_2 + \rho_1)} g_p, \quad (22a)$$

$$\gamma_0^2 = \frac{\ell}{R} \frac{(\rho_2 - \rho_1)}{(\rho_2 + \rho_1)} g_p, \quad (22b)$$

and

$$\gamma_0^2 = \frac{\ell(\ell+1)}{R} \frac{(\rho_2 - \rho_1)}{[\ell\rho_2 + (\ell+1)\rho_1]} g_p \quad (22c)$$

for the three geometries. Equation (22a) is the familiar “classical” RT growth rate for incompressible planar flow. The spherical results [Eqs. (20c) and (22c)] are equivalent to the result of Plesset⁸ for incompressible fluid ($\gamma_\rho = 0$), even though they are not easily recognized as such. For the special case of a free surface (either $\rho_1 = 0$ or $\rho_2 = 0$), Eqs. (20) and (22) become Bell’s⁷ final result.

The driving terms are easily identified as being the only terms containing either an acceleration or a density jump, both of which are required for the buoyant force driving the RT effect. Compared with alternative formulations,^{8,11} Eqs. (20) and (22) display a more physically meaningful isolation of the RT effect into a single term. Even though the RT effect can be

isolated in this way, the total perturbation growth rates do not separate naturally into RT and BP contributions. The form of Eqs. (20) does allow equations governing accelerationless growth to be obtained by setting $\gamma_0 = 0$, but the accelerationless limit cannot be simply combined with the classical RT growth rate to obtain a correct result.

Equations (20) are easily solved over time intervals where the compression and convergence rates, γ_ρ and γ_R , respectively, and the RT growth rate γ_0 are constant. The resulting solution pairs are exponential in time with constant growth rates,

$$\gamma_\pm = \frac{1}{2} \gamma_\rho \pm \sqrt{\gamma_0^2 + \frac{1}{4} \gamma_\rho^2} \quad (23a)$$

for both planar and cylindrical geometry and

$$\gamma_\pm = \frac{1}{2} (\gamma_\rho + \gamma_R) \pm \sqrt{\gamma_0^2 + \frac{1}{4} (\gamma_\rho + \gamma_R)^2} \quad (23b)$$

for spherical geometry. Since γ_0^2 can be negative, the growth rates can be complex, giving perturbations exhibiting exponential or sinusoidal behavior, or both. In characterizing an interface as stable or unstable, Plesset argues that exponential behavior suggests unbounded growth of one of the solutions, which indicates instability. Conversely, oscillation suggests stability. Even though Eqs. (20c) and (22c) are consistent with the corresponding equations of Plesset,⁸ one can draw different conclusions about the criteria for stability based solely on the inspection of the respective equations. Except for the case of planar incompressible flow, exponential growth, for example, does not necessarily imply net growth. Equations (23) can be a guide in formulating general stability criteria for intervals where γ_ρ , γ_R , and γ_0 are constant, but there are other approaches. In the next section where BP effects in the large- γ_0 limit are considered, the solutions appear as products of power-law factors of R and ρ and a factor that is exponential in $\gamma_0 t$. If one does not regard power-law density and radius scaling behavior as either stable or unstable, then the question of stability is simply the question of the sign of γ_0^2 , without regard for BP effects.

Solving fully time-dependent perturbation equations [Eqs. (20) and (22)] provides a more complete and thus more correct description of RT growth than the common practice of

estimating unstable growth from an exponential growth factor, such as

$$a(t) = a(0) \exp \left[\int_0^t \gamma(t') dt' \right], \quad (24)$$

where the positive growth rate is used in the integrand. The fully time-dependent solution permits specifying amplitudes with arbitrary initial values and time derivatives, while the growth factor implies a particular initial condition. For example, the solution pair for incompressible planar flow has equal and opposite growth rates, so a solution with a static initial amplitude is composed initially of equal parts of the growing and decaying components of the general solution. Equation (24), on the other hand, attributes the entire initial amplitude to the growing component of the full solution. As a result, the growth-factor solution will become too large by a factor of 2 if it is used to represent growth of a perturbation that is initially static. More generally, if the acceleration changes abruptly from one constant value to another, matching the solutions before and after the change cannot be done without considering the fully time-dependent solution. A second advantage of the fully time-dependent formulation is that Richtmyer–Meshkov-like¹³ behavior is obtained for impulsive acceleration. For an acceleration with an appropriate oscillating component, the fully time-dependent formulation exhibits the dynamic stabilization effect obtained by Betti *et al.*,¹⁴ another effect that cannot be described by an exponential growth factor.

Equations (20) and (22) were originally derived for use in a perturbation growth model for a saturable multimode model of RT instability¹⁶ applicable to simulations of inertial confinement fusion experiments.¹⁵

Scaling

In this section, we shall examine both the mass and spatial perturbation amplitudes in two limits where the BP effects appear entirely as scaling factors with power-law dependences on the interface density and radius. The first is the accelerationless limit of small γ_0 , and the second is the limit of rapid RT growth, relative to the compression and convergence rates. As will be shown below, the accelerationless BP effects are different from BP effects occurring in combination with the RT instability.

In the limit where the interface acceleration vanishes, or when the density jump at the interface vanishes, γ_0 approaches

zero. In this limit, assuming constant compression and convergence rates, the pairs of solutions are of the form $z_{\pm} \propto \exp(\gamma_{\pm} t)$, where

$$\gamma_{\pm} = [\gamma_{\rho}, 0] \quad (25a)$$

for both planar and cylindrical geometry and

$$\gamma_{\pm} = [\gamma_{\rho} + \gamma_R, 0] \quad (25b)$$

for spherical geometry. The leading-order RT corrections to Eqs. (25) are second order in γ_0 . From assuming that γ_{ρ} and γ_R are constants, we have $R \propto \exp(\gamma_R t)$ and $\rho \propto \exp(\gamma_{\rho} t)$ and the solution pairs are

$$z_{\pm} \propto [\rho, 1] \quad (26a)$$

for planar and cylindrical geometry and

$$z_{\pm} \propto [\rho R, 1] \quad (26b)$$

for spherical geometry. For uniform compression of a constant cylindrical mass $M = \rho R^2$ or spherical mass $M = \rho R^3$, the solutions $z_{M\pm}$ are

$$z_{M\pm} = [R^{-2}, 1] \quad (27)$$

for both cylindrical and spherical geometry. The spatial amplitudes are related to the mass amplitudes according to Eq. (21), which gives

$$a_{\pm} = [1, \rho^{-1}], \quad (28a)$$

$$a_{\pm} = [R^{-1}, (\rho R)^{-1}], \quad (28b)$$

and

$$a_{\pm} = [R^{-1}, (\rho R^2)^{-1}]. \quad (28c)$$

For uniform compression of a constant cylindrical mass or spherical mass, the solutions $a_{M\pm}$ are

$$a_{M\pm} = [R^{-1}, R] \quad (29)$$

for both cylindrical and spherical geometry.

While the accelerationless limit gives a view of the BP effects in the absence of RT growth, a more interesting limit is that of a dominant RT effect or, equivalently, of large ℓ where we have $\gamma_0 \gg \gamma_\rho$, $\gamma_0 \gg \gamma_R$, and $\gamma_0^2 \gg \dot{\gamma}_0$. In this limit, Eqs. (23) become, to leading order in the small numbers γ_ρ/γ_0 and/or γ_R/γ_0 ,

$$\gamma_\pm \approx \frac{1}{2} \gamma_\rho \pm \gamma_0 \quad (30a)$$

for both planar and cylindrical geometry and

$$\gamma_\pm \approx \frac{1}{2} (\gamma_\rho + \gamma_R) \pm \gamma_0 \quad (30b)$$

for spherical geometry. In an imploding sphere, such as in the deceleration phase of an ICF implosion experiment,^{17,18} for example, we estimate the magnitude of the small parameter of this limit by writing the classical growth rate as

$$\gamma_0^2 \approx \ell A \frac{\ddot{R}}{R}, \quad (31)$$

where A is the Atwood number

$$A \equiv \frac{(\rho_2 - \rho_1)}{(\rho_2 + \rho_1)}. \quad (32)$$

For the purpose of characterizing a large- ℓ limit, it is sufficient to assign a single time scale τ to all time derivatives,

$$\ddot{R} \sim R/\tau^2, \quad \dot{R} \sim R/\tau, \quad \dot{\rho} \sim \rho/\tau, \quad (33)$$

so that the small number in this limit is

$$\gamma_\rho/\gamma_0 \sim \gamma_R/\gamma_0 \sim (\ell A)^{-1/2}, \quad (34)$$

which is small for the large mode numbers of interest in ICF implosions.¹⁷ In this limit, the solution pairs are

$$z_\pm \propto \rho^{1/2} e^{\pm \gamma_0 t} \quad (35a)$$

for planar and cylindrical geometry and

$$z_\pm \propto \rho^{1/2} R^{1/2} e^{\pm \gamma_0 t} \quad (35b)$$

for spherical geometry. For uniform compression of a constant cylindrical mass or spherical mass, the solutions $z_{M\pm}$ are

$$z_{M\pm} = R^{-1} e^{\pm \gamma_0 t} \quad (36)$$

for both cylindrical and spherical geometry. The corresponding spatial amplitudes are

$$a_\pm = \rho^{-1/2} e^{\pm \gamma_0 t}, \quad (37a)$$

$$a_\pm = \rho^{-1/2} R^{-1} e^{\pm \gamma_0 t}, \quad (37b)$$

and

$$a_\pm = \rho^{-1/2} R^{-3/2} e^{\pm \gamma_0 t}. \quad (37c)$$

For uniform compression of a constant cylindrical mass or spherical mass, the solutions $a_{M\pm}$ are

$$a_{M\pm} = e^{\pm \gamma_0 t}, \quad (38)$$

which is an interesting example of a spatial amplitude evolving virtually free of any BP effects.

In this large- ℓ limit, the BP effects appear separately from the RT growth factors as scaling factors in powers of ρ and/or R that are the same for both solutions of each pair. The fact that the BP effects are the same for both solutions is a property unique to the large- ℓ limit. Except in this one limit, Eqs. (23) predict different BP effects for the two solutions.

Discussion

In the accelerationless limit where $\gamma_0 = 0$, the density and radius scaling of the perturbation solutions of constant mass amplitude are readily visualized. These solutions are the second solutions of Eqs. (26) and (27) and their spatial-amplitude

counterparts in Eqs. (28) and (29). The spherical cases are illustrated schematically in Fig. 94.17, where a layer of fluid is highlighted to suggest the “peak-to-valley” extent of the perturbation. Figure 94.17(a) shows an incompressible spherical layer thickening as it converges to maintain constant density, and Fig. 94.17(b) shows the same layer compressing in proportion to the radius of the uniformly compressing homogeneous sphere in which it is embedded. It is important to remember that this solution of constant mass amplitude is obtained only with appropriate initial conditions. The general solution for arbitrary initial conditions exhibits a more complicated mixture of behaviors. The fact that the convergence and compression effects are different for the two solutions in each pair is the rule, not the exception. It is a unique property of the opposite limit, where the RT rate is much larger than the compression and convergence rates, that both solutions exhibit the same BP scaling with density and radius.

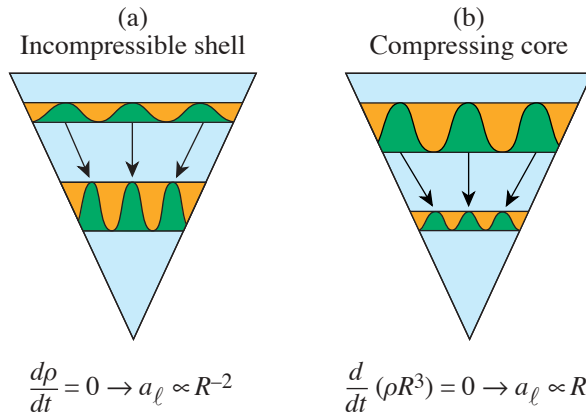


Figure 94.17

The cases of a perturbed surface embedded in an incompressible shell and a compressible sphere suggest, respectively, $a_\ell \propto R^{-2}$ and $a_\ell \propto R$ scaling of the spatial amplitude in the absence of a Rayleigh–Taylor growth term. Each of these solutions are paired with another independent solution, however, and the scaling behavior is more complicated if contributions from these other solutions are introduced by the initial conditions of the amplitude.

A simple demonstration of the importance of BP effects and the differences obtained from alternative initial conditions are shown in Fig. 94.18. The two plots show the growth of the spatial amplitude of a perturbation of an imploding, decelerating spherical interface. The implosion parameters correspond roughly to those of ICF capsule implosions near peak compression. The surface is assumed to compress by a radial factor of 10 while decelerating uniformly at $2.0 \times 10^{16} \text{ cm/s}^2$ from a radius of $400 \mu\text{m}$. The perturbation growth was calculated by direct integration of Eq. (20c). Each plot shows the amplitude

growth for an incompressible spherical shell ($\gamma_\rho = 0$), for a uniformly compressing sphere ($3\gamma_R + \gamma_\rho = 0$), and for the incompressible planar limit ($\gamma_R = \gamma_\rho = 0$) with no BP effects. Figure 94.18(a) shows results obtained by applying a static initial condition to the spatial amplitude, and Fig. 94.18(b) shows the same results obtained by applying a static initial condition to the mass amplitude. The RT growth rate was set to $\gamma_0^2 = 4\ddot{R}/R$, choosing $\ell A = 4$ to create an intermediate case between the accelerationless and the large-growth limits. The results show that BP effects vary in importance, depending on which compressibility assumption is made, and that they are sensitive to the choice of initial condition. If the amplitude is initialized as a static mass amplitude, the incompressible shell growth is particularly large. These results should not be ex-

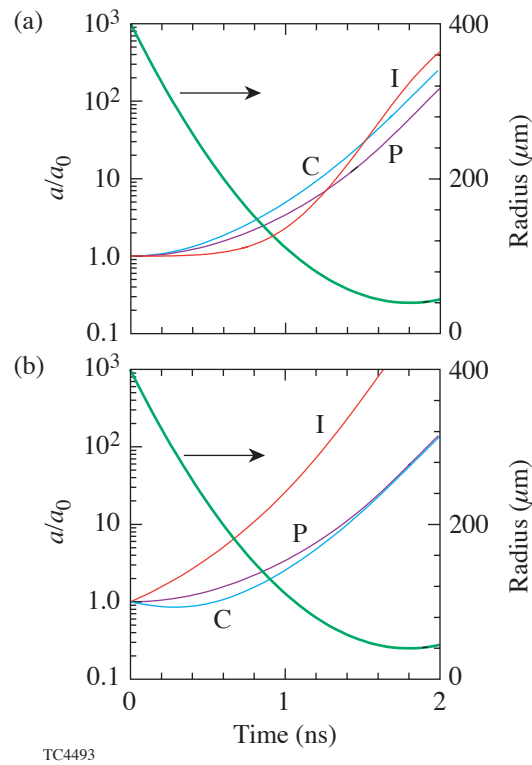


Figure 94.18

Significant differences in perturbation growth are obtained for different compressibility cases and with different initializations. Results for perturbations of an incompressible shell (I) and a compressible sphere (C) are shown, compared with the results of the “classical” Rayleigh–Taylor model, or the incompressible planar approximation (P), where convergence and compression effects are ignored. The importance of initial conditions is seen by comparing results obtained using (a) static initial spatial amplitudes and (b) static initial mass amplitudes.

pected to conform closely to the scaling results [Eqs. (37c) and (38)] because the compression, convergence, and RT rates are not constant and γ_0^2 does not occur close to either of the scaling limits of the previous section, but Eq. (38) does suggest that the amplitudes from the compressible sphere and incompressible planar models should tend to agree as they seem to do in both plots. Also, Eq. (37c) suggests that the BP effect on the amplitude of a spatial perturbation of a spherical surface converging by a factor of 10 should increase the amplitude over the other two cases by about 1.5 decades, which is approximately what is seen in Fig. 94.18(b).

Actual ICF implosions are, of course, more complicated than this simple illustration. The deceleration of the compressing core occurs during a brief “deceleration” phase following a longer “coasting” phase between the period of acceleration due to the driver and the onset of deceleration by the compressing core. The coasting phase can be characterized crudely by an incompressible shell in the accelerationless limit ($\gamma_p=0$ and $\gamma_0=0$), and the deceleration phase would resemble, in contrast, the case of the uniformly compressing sphere ($3\gamma_R+\gamma_p=0$). In a realistic simulation, the convergence and compression rates vary continuously, and the true description of an unstable surface will be somewhere between the limits of an incompressible shell and a uniformly compressible sphere of constant mass.

Overall, BP effects in the accelerationless limit and in the limit where the RT growth is dominant exhibit distinct differences in the nature of the effects and in their importance. Between these two scaling limits, the latter is the more applicable limit when analyzing observations of hydrodynamic instability in ICF implosion experiments.

The BP effects have been called the “Bell–Plesset instability,”⁶ which is not a correct description. They may be better described as a scaling behavior, for example, but they are certainly not a true instability in the sense that the RT instability is a true instability whose growth is driven by positive feedback that grows in proportion to its amplitude.

Summary and Conclusion

A formal description of the BP effects of compression and geometric convergence on the RT instability has been obtained. Even though the chosen model is restricted to incompressible perturbations of an interface separating homogeneous fluids and to a spatially uniform compression rate for the entire fluid, the model is general enough to encompass a usefully broad range of behavior. Results for three geometries (planar,

cylindrical, and spherical) are presented in parallel, and the fluid is allowed to compress and converge independently. The governing perturbation equations [Eqs. (20) and (22)] are only slightly modified from the classical RT equations as given by Eqs. (20a) and (22a) for incompressible ($\gamma_p=0$) planar flow whose solutions exhibit simple exponential or sinusoidal evolution of the interface distortion. The RT growth rates for the three chosen geometries are very similar and, as expected, become identical in the limit of large harmonic order ℓ or k , where $k=\ell/L$. The first of two modifications of the planar incompressible RT equation that add the BP effects is to write it in terms of a mass amplitude. It is not surprising that the perturbation equations would be simplified by writing them in terms of a mass amplitude because an embedded perturbed interface would simply compress and converge with the flow, with the peak-to-valley displacement of the interface demarcating a layer of constant mass. The second modification is to add a first-time-derivative term appropriate for the chosen geometry, which results in a pair of growth rates that differ by more than just a sign flip.

With constant compression, convergence, and growth rates, the simple form of Eqs. (20) leads to BP effects expressible as power-law scaling with density and radius. These scalings vary, depending on the underlying geometry, the assumed interdependence of the compression and convergence rates, and which limit of either slow [Eqs. (25)–(29)] or rapid [Eqs. (30)–(33)] RT growth applies. In the limit of slow RT growth or, equivalently, in the limit of true accelerationless growth, each solution in a pair has its own distinct BP scaling, and only one solution of the pair exhibits the constant mass amplitude expected for an embedded surface. The scaling behavior is distinctly different for RT growth that is much faster than the convergence and/or compression. While rapid RT growth might amount to several e foldings in, for example, an ICF implosion, the BP effects can be much smaller and still amount to a significant effect. In this limit, the BP scaling becomes identical for each of the pair of solutions. While the variety of scalings among the solutions is simpler where RT growth dominates, the scaling is neither as intuitive nor as recognizable as the constant mass amplitude solution of the accelerationless limit. Perhaps the most surprising result is Eq. (38), indicating no first-order BP effect at all for the uniform compression of a constant spherical or cylindrical mass.

Even though the underlying assumptions behind the results shown here are somewhat restrictive, this presentation of a unified body of results for several geometries and flow characteristics hopefully has conveyed a clearer sense of the origin,

nature, and the surprising diversity of BP effects and their tendency to defy any simple characterization applicable over a wide range of circumstances.

ACKNOWLEDGMENT

This work was supported by the U.S. Department of Energy Office of Inertial Confinement Fusion under Cooperative Agreement No. DE-FC03-92SF19460, the University of Rochester, and the New York State Energy Research and Development Authority. The support of DOE does not constitute an endorsement by DOE of the views expressed in this article.

REFERENCES

1. Lord Rayleigh, Proc. London Math Soc. **XIV**, 170 (1883).
2. G. Taylor, Proc. R. Soc. London Ser. A **201**, 192 (1950).
3. S. Chandrasekhar, *Hydrodynamic and Hydromagnetic Stability*, International Series of Monographs on Physics (Dover Publications, New York, 1981), Chap. X, pp. 428–480.
4. L. D. Landau and E. M. Lifshitz, *Fluid Mechanics* (Pergamon Press, London, 1959).
5. J. B. Beck, “The Effects of Convergent Geometry on the Ablative Rayleigh–Taylor Instability in Cylindrical Implosions,” Ph.D. thesis, Perdue University, 1996.
6. W. W. Hsing and N. M. Hoffman, Phys. Rev. Lett. **78**, 3876 (1997).
7. G. I. Bell, Los Alamos National Laboratory, Report LA-1321 (1951).
8. M. S. Plesset, J. Appl. Phys. **25**, 96 (1954).
9. W. W. Hsing *et al.*, Phys. Plasmas **4**, 1832 (1997).
10. V. N. Goncharov, P. McKenty, S. Skupsky, R. Betti, R. L. McCrory, and C. Cherfils-Clérouin, Phys. Plasmas **7**, 5118 (2000).
11. P. Amendt *et al.*, Phys. Plasmas **10**, 820 (2003).
12. A. L. Fetter and J. D. Walecka, *Theoretical Mechanics of Particles and Continua*, International Series in Pure and Applied Physics (McGraw-Hill, New York, 1980).
13. R. D. Richtmyer, Commun. Pure. Appl. Math. **XIII**, 297 (1960).
14. R. Betti, R. L. McCrory, and C. P. Verdon, Phys. Rev. Lett. **71**, 3131 (1993).
15. R. Epstein, J. A. Delettrez, and C. P. Verdon, presented at the 27th Annual Anomalous Absorption Conference, Vancouver, BC, Canada, 1–5 June 1997.
16. S. W. Haan, Phys. Rev. A **39**, 5812 (1989).
17. P. W. McKenty, V. N. Goncharov, R. P. J. Town, S. Skupsky, R. Betti, and R. L. McCrory, Phys. Plasmas **8**, 2315 (2001).
18. D. D. Meyerhofer, J. A. Delettrez, R. Epstein, V. Yu. Glebov, V. N. Goncharov, R. L. Keck, R. L. McCrory, P. W. McKenty, F. J. Marshall, P. B. Radha, S. P. Regan, S. Roberts, W. Seka, S. Skupsky, V. A. Smalyuk, C. Sorce, C. Stoeckl, J. M. Soures, R. P. J. Town, B. Yaakobi, J. Frenje, C. K. Li, R. D. Petrasso, F. H. Séguin, K. Fletcher, S. Padalino, C. Freeman, N. Izumi, R. A. Lerche, T. W. Phillips, and T. C. Sangster, Plasma Phys. Control. Fusion **43**, A277 (2001).